BJP BRITISH JOURNAL OF PHARMACOLOGY

BPS BRITISH PHARMACOLOGICAL SOCIETY

British Journal of Pharmacology (2010), 160, 1016–1028

0007-1188/10
www.brjpharmacol.org

RESEARCH PAPER

Kinetic analysis of novel mono- and multivalent VHH-fragments and their application for molecular imaging of brain tumours

U Iqbal[1]*, U Trojahn[2]*, H Albaghdadi[1,3], J Zhang[1], M O'Connor-McCourt[4], D Stanimirovic[1,3], B Tomanek[5,6], G Sutherland[5,6] and A Abulrob[1,3]

[1]*Institute for Biological Sciences, National Research Council of Canada, Ottawa, Ontario, Canada,* [2]*Department of Biochemistry, McGill University, Montreal, Quebec, Canada,* [3]*Department of Cellular and Molecular Medicine, Faculty of Medicine, University of Ottawa, Ottawa, Ontario, Canada,* [4]*Biotechnology Research Institute, National Research Council of Canada, Montreal, Quebec, Canada,* [5]*Institute for Biodiagnostics (West), National Research Council of Canada, Calgary, Alberta, Canada, and* [6]*Department of Clinical Neurosciences, University of Calgary, Calgary, Alberta, Canada*

Background and purpose: The overexpression of epidermal growth factor receptor (EGFR) and its mutated variant EGFRvIII occurs in 50% of glioblastoma multiforme. We developed antibody fragments against EGFR/EGFRvIII for molecular imaging and/or therapeutic targeting applications.
Experimental approach: An anti–EGFR/EGFRvIII llama single-domain antibody (EG_2) and two higher valency format constructs, bivalent EG_2-hFc and pentavalent V2C-EG_2 sdAbs, were analysed *in vitro* for their binding affinities using surface plasmon resonance and cell binding studies, and *in vivo* using pharmacokinetic, biodistribution, optical imaging and fluorescent microscopy studies.
Key results: Kinetic binding analyses by surface plasmon resonance revealed intrinsic affinities of 55 nM and 97 nM for the monovalent EG_2 to immobilized extracellular domains of EGFR and EGFRvIII, respectively, and a 10- to 600-fold increases in apparent affinities for the multivalent binders, V2C-EG_2 and EG_2-hFc, respectively. *In vivo* pharmacokinetic and biodistribution studies in mice revealed plasma half-lives for EG_2, V2C-EG_2 and EG_2-hFc of 41 min, 80 min and 12.5 h, respectively, as well as a significantly higher retention of EG_2-hFc compared to the other two constructs in EGFR/EGFRvIII-expressing orthotopic brain tumours, resulting in the highest signal in the tumour region in optical imaging studies. Time domain volumetric optical imaging fusion with high-resolution micro-computed tomography of microvascular brain network confirmed EG_2-hFc selective accumulation/retention in anatomically defined tumour regions.
Conclusions: Single domain antibodies can be optimized for molecular imaging applications by methods that improve their apparent affinity and prolong plasma half-life and, at the same time, preserve their ability to penetrate tumour parenchyma.
British Journal of Pharmacology (2010) **160,** 1016–1028; doi:10.1111/j.1476-5381.2010.00742.x

Keywords: molecular imaging; multivalency; epidermal growth factor receptor; single domain antibody; brain cancer; surface plasmon resonance

Abbreviations: EGFR, epidermal growth factor receptor; EGFRvIII, class III mutant EGFR; GBM, glioblastoma multiforme; sdAb, single-domain antibody; SPR, surface plasmon resonance

Introduction

Glioblastoma multiforme (GBM), or World Health Organization grade IV astrocytoma, is the most malignant type of brain neoplasm with an average patient survival of about 15 months under the current treatment regime (Strupp *et al.*, 2005). GBM is a highly invasive and angiogenic tumour that produces heterogeneous vessels, some of which are large, porous and exhibit abnormalities in the blood-brain barrier (Vajkoczy *et al.*, 1998). It is through these 'leaky' vessels that molecular agents can penetrate into the tumour region to interact with tumour cell-specific targets. The tumour microenvironment, characterized by reduced tumour blood flow and increased intratumoural pressure (Blasberg and Groothius, 1986; Jain, 1994), as well as the

Correspondence: Dr Abedelnasser Abulrob, Institute for Biological Sciences, National Research Council of Canada, 1200 Montreal Road, Ottawa, Ontario, Canada K1A 0R6. E-mail: abedelnasser.abulrob@nrc.gc.ca
*These authors contributed equally to this work.
Received 10 November 2009; revised 19 January 2010; accepted 17 February 2010

presence/up-regulation of drug efflux transporters at the blood-tumour barrier (De Vries *et al*., 2006), further complicates the delivery of exogenous molecules to and within tumour parenchyma.

EGFR is a receptor tyrosine kinase that plays an important role in tumourigenesis including processes of cell survival, proliferation and angiogenesis (Nicholas *et al*., 2006). While the normal brain exhibits low EGFR expression (Liu *et al*., 2003), the EGFR is highly expressed in approximately 50% of GBM patients due to gene amplification (Libermann *et al*., 1985). Mutations of the EGFR gene, including an in-frame deletion of 801 bp in exons 2–7 (type III mutation), are often associated with EGFR gene amplification. This leads to the expression of a class III mutant EGFR (EGFRvIII), characterized by constitutive autophosphorylation of the tyrosine kinase domain resulting in a ligand-independent receptor (Wikstrand *et al*., 1998). The appearance of EGFRvIII is associated with poor tumour prognosis (Shinojima *et al*., 2003).

The EGFR and EGFRvIII have been exploited as targets for molecular imaging and therapeutic applications in a variety of human cancers (Laskin and Sandler, 2004). In recent years several IgG antibodies against EGFR, including cetuximab, have proved successful at therapeutic targeting of the EGFR in clinical trials for peripheral tumours such as head and neck cancer and metastatic colorectal cancer (Blick and Scott, 2007). The same antibody is currently undergoing clinical trials for recurrent GBM (Belda-Iniesta *et al*., 2006); however, it is generally believed that delivery to the brain tumour remains the major obstacle limiting usefulness of antibody treatment for GBM (Stragliotto *et al*., 1996).

Although intact IgG antibody molecules have proved partially successful in various therapeutic applications (Blick and Scott, 2007), they have had limited application in molecular imaging due to their relatively slow clearance from the circulation and tissues resulting in limited imaging contrast early after injection, high background signal and non-uniform tumour penetration (Schier *et al*., 1996). This limitation can be overcome by developing antibody fragments such as single-chain (scFv) and single-domain antibodies (sdAb) engineered to maximize specific binding to the targeted tumour and achieve fast blood clearance and appropriate pharmacokinetics. sdAbs are derived from the variable regions of camelid heavy-chain antibodies (Hamers-Casterman *et al*., 1993) and have a molecular weight of 12–15 kDa, low nanomolar affinities when isolated from an immune library (Arbabi Ghahroudi *et al*., 1997), and high temperature and protease stability. These antibody fragments have been engineered into a variety of antibody constructs displaying polyvalency and bi-specificity (Conrath *et al*., 2001; Zhang *et al*., 2004). Their small molecular size, lack of the immunoglobulin Fc region (C_H2-C_H3) and moderate affinities can be either beneficial or limiting factors depending on the desired application. Since sdAbs in monovalent (native) form are rapidly cleared from the circulation due to kidney filtration, for *in vivo* targeting it is generally desirable to increase their apparent size to over 65 kDa to bypass kidney filtration. This can be achieved by various antibody engineering strategies, such as pegylation, multimerization, fusion to other antibody fragments or creation of bi-specific sdAbs, where one of the fragments binds a plasma 'carrier' such as albumin (Roovers *et al*., 2007).

In this study, a recently developed sdAb cross-reactive against EGFR and EGFRvIII (named EG_2), was engineered to increase valency and circulation half-life using two strategies: (i) pentamerization by fusing five EG_2 molecules with the verotoxin B multimerization domains (Zhang *et al*., 2004) resulting in a 128 kDa construct, V2C- EG_2; and (ii) fusion of two EG_2 molecules to the human Fc fragment resulting in a bivalent, 80 kDa construct, EG_2-hFc (Zhang *et al*., 2009). These constructs were analysed *in vitro* for their kinetic binding properties to EGFR and EGFRvIII and evaluated *in vivo* for their pharmacokinetic properties and the ability to target orthotopic glioblastoma tumours expressing EGFR/EGFRvIII for *in vivo* imaging applications. It was found that EG_2-hFc displayed optimum binding and pharmacokinetic properties that enabled improved glioblastoma targeting and retention, and excellent signal-to-noise ratio for *in vivo* imaging applications.

Methods

Expression and purification of proteins

Human EGFR extracellular domain (EGFR-ECD) was produced in Sf9 cells and purified by two-step ion-exchange chromatography as reported previously (Brown *et al*., 1994). The production and purification of EGFRvIII-ECD was carried out as described by Campa *et al*. (2000). Isolation of EG_2 sdAb was achieved by llama immunization with EGFRvIII-ECD, construction of an immune phage display library and subsequent panning as previously described (McCafferty *et al*., 1990). Pentamerization of EG_2 into V2C-EG_2 was achieved by fusion to verotoxin subunit B1 (Zhang *et al*., 2004; Abulrob *et al*., 2005). EG_2-hFc was constructed by fusion of EG_2 camelid single-domain antibody to the human Fc fragment and expressed in a HEK293 expression system as described previously (Zhang *et al*., 2009). Figure 1 shows a schematic representation of the different multivalent EG_2 antibody fragments used in the study.

Cell culture

The human glioblastoma parental cell line U87MG and its sublines U87MG.wtEGFR and U87MG.EGFRvIII, which overexpress wild-type EGFR and the EGFR type III variant (EGFRvIII), respectively, were a kindly provided by Dr W.L Cavenee (Ludwig Institute for Cancer Research, La Jolla, CA, USA). Cell lines were cultured and maintained as described previously (Abulrob *et al*., 2004).

Analysis of binding kinetics by surface plasmon resonance

The binding kinetics of the different EG_2 sdAb constructs were analysed by surface plasmon resonance (SPR) using a Biacore3000 optical sensor platform equipped with research-grade CM5 sensor (GE Healthcare Bio-Sciences Corp., Piscataway, NJ). Purified proteins (EGFR, EGFRvIII, EG_2, V2C-EG_2 and EG_2-hFc) were immobilized on the sensor chip surface of a carboxylated dextran-coated gold film using the standard amine coupling kit following the manufacturer's protocol. Briefly, 70 μL of a mixed solution of NHS/EDC (1:1,

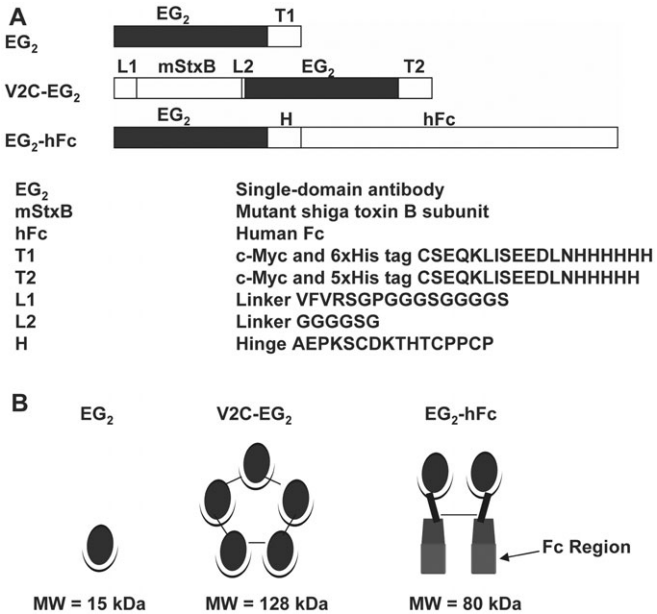

Figure 1 (A) Linear representation of the primary structure and (B) two-dimensional illustration of the monomeric EG_2, pentavalent V2C EG_2 and bivalent EG_2-hFc sdAbs used in this study.

v/v) were injected to activate the carboxylated dextran, followed by manual injection of protein in 10 mM NaOAc (pH 4.5) until the desired surface density was reached. Ethanolamine 1 M in water (pH 8.5) was then injected to de-activate residual NHS-esters on the sensor chip. All binding experiments were carried out in HEPES buffer (10 mM HEPES, 150 mM NaCl, 3.4 mM EDTA, 0.005% Tween 20, pH 7.4) at 25°C. Antibodies or receptor ectodomains at concentrations between 3.9 and 500 nM were injected randomly over the receptor ectodomain or antibody surfaces, respectively, at a flow rate of 20 $\mu L \cdot min^{-1}$ unless otherwise stated. After each injection, the surfaces were regenerated with two 30 s injections of 10 mM HCl. The resulting sensorgrams were aligned and double referenced using a mock activated surface and blank buffer injections. Kinetic data were evaluated by globally fitting the sensorgrams to a simple 1:1 interaction model using the Biacore software BiaEvaluation version 4.1 (GE Healthcare Bio-Sciences Corp.). The equilibrium K_Ds were determined from the resulting kinetic association and dissociation rates (k_d/k_a), and a minimum of nine independent runs were used to generate the reported standard deviations.

Affinity labelling of cell surface EGFR or EGFRvIII with ^{125}I-EG_2

Radiolabelling of EG_2 sdAb was carried out using the [^{125}I]-Bolton-Hunter reagent (PerkinElmer Life Sciences, Boston, MA, USA), as described previously (Bolton and Hunter, 1973). For cell binding experiments, 5×10^5 cells were seeded in duplicate wells in gelatin-coated six-well plates and allowed to adhere for 48 h. [^{125}I]-EG_2 25 nM was added to the wells either treated or untreated with 2.5 μM unlabelled EG_2. Plates were incubated for 2 h at 4°C. sdAbs were crosslinked with 1 mM freshly prepared BS3 (Pierce, Rockford, IL, USA) for 5 min. Cells were dissolved and cell lysates were separated in 6% SDS-PAGE. The dried gel was exposed to a phosphorimage plate for at least 48 h, which was then scanned with a Typhoon Trio+ variable mode scanner (Amersham Biosciences, Uppsala, Sweden) using the storage phosphor mode.

[^{125}I]-EG_2 competition binding assay

U87MG.EGFRvIII and U87MG.wtEGFR cells, 4×10^4, were seeded in each well on gelatin-coated 48-well plates (Corning Incorporated, NY, USA) and grown in complete media for 48 h. Wells were then washed twice with complete PBS (PBS with 0.9 mM $CaCl_2$, 0.49 mM $MgCl_2$)/0.1% BSA and incubated with [^{125}I]-EG_2 (20 nM) and serial dilutions of unlabelled EG_2 (0.01–10 μM) for 2 h at 4°C. After three more washes with complete PBS, the cells were dissociated for 30 min in solubilizaton buffer (20 mM Tris, 1 mM EDTA, 10% (v/v) glycerol, 1% (v/v) Triton-X-100, pH 7.4) and transferred into plastic vials. The amount of radioactivity was counted in an automatic gamma counter (Wallac Wizard 1470, PerkinElmer Life). The resulting data points were fitted applying nonlinear regression to a one-site binding model using the GraphPad Prism software (La Jolla, CA, USA).

Pharmacokinetic analysis

EG_2, EG_2-hFc and V2C-EG_2 sdAbs were labelled with cy5.5 succinimidyl ester using methods recommended by the manufacturer (GE Healthcare). Labelling was optimized such that each sdAb had a dye/antibody ratio of two. One milligram of EG_2-cy5.5, EG_2-hFc-cy5.5 or V2C-EG_2-cy5.5 sdAb was injected via the tail vein in normal CD-1 mice. Blood samples of 25 μL were collected by creating a small nick in the tail vein followed by collection of blood in a heparin-treated tube. Blood samples were collected at multiple time points at 5 min, 30 min, 1 h, 1.5 h, 2 h, 4 h and 24 h after injection. Samples were analysed for labelled antibodies using a fluorescent plate reader with excitation 670 nm and emission 690 nm and compared to a standard curve of a range of concentrations of the labelled antibodies diluted in blood. Pharmacokinetic parameters were calculated using the WinNonlin pharmacokinetic software package (Pharsight Corporation, Mountain View, CA, USA). A two-compartment, IV-Bolus model was selected for pharmacokinetic modelling, as it best represented the actual data. This model is described by the following equation: $C(t) = A \exp(-\alpha t) + B \exp(-\beta t)$, where $C(t)$ represents the concentration of agent in serum. A and B represent the zero time intercept of the alpha phase and beta phase, respectively, and α and β are disposition rate constants, $\alpha > \beta$. The area under the serum concentration–time curve was calculated with the equation $AUC_{0-\infty} = D/V/K_{10}$, where D is dose given, V is apparent distribution volume and K_{10} is elimination rate constant. Total clearance was determined from the equation $Cl/F = D/AUC_{0-\infty}$.

Intracranial model of U87MG.EGFRvIII glioblastoma in nude mice

For the animal model of high-grade glioma, the U87MG.EGFRvIII cell line, which overexpresses EGFRvIII (and has a lower level of wtEGFR, similar to the parental cell

line), was used to evaluate the EG_2 antibody isolated from the EGFRvIII-ECD-immunized llama phage-display library. Cells were brought into suspension at a final concentration of 1×10^4 cells·μL^{-1} PBS and were kept on ice until injection. For intracerebral stereotactic implantation of U87MG.EGFRvIII, CD-1 nude mice (male, 6–8 weeks old) were purchased from Charles River Canada. First, mice underwent isofluorane deep anaesthesia, and the scalp was swabbed with iodine and alcohol. The skin was incised and a 10 μL syringe was used to inoculate 5 μL of U87MG.EGFRvIII cell suspension into the corpus striatum in the right hemisphere (3.0 mm deep; 1 mm anterior and 2 mm lateral to the bregma). The skin was sutured with three knots, followed by application of tissue glue and local analgesia. The animals developed solid, spherical tumours for 10 days that were large enough to be detected by MRI (1.2–2.9 $mm^3 \pm 0.3$), at which point *in vivo* studies started. The animal experiments were all carried out in accordance with the National Research Council of Canada – Institute for Biological Sciences Animal Care Committee.

In vivo *near-infrared fluorescence imaging of mice bearing U87MG.EGFRvIIII brain tumours*

One nanomole of each labelled antibody was injected via the tail vein in mice bearing 10 day old U87MG.EGFRvIII brain tumours. *In vivo* imaging studies were performed using a small-animal time-domain eXplore Optix MX2 pre-clinical imager (Advanced Research Technologies, Montreal, QC) as described previously (Abulrob *et al*., 2007; 2008) at 1, 4, 24, 48 and 72 h after injection. For imaging, mice were first anaesthetized with isofluorane, and then positioned on an animal stage in a chamber that allows for maintenance of gaseous anaesthesia. In all imaging experiments, a 670 nm pulsed laser diode with a repetition frequency of 80 MHz and a time resolution of 12 ps light pulse was used for excitation. The fluorescence emission at 700 nm was collected by a highly sensitive time-correlated single photon counting system and detected through a fast photomultiplier tube. The data were recorded as temporal point-spread functions and the images were reconstructed as fluorescence concentration maps using ART Optix Optiview analysis software 2.0 (Advanced Research Technologies, Montreal, QC, Canada).

Microfil-enhanced X-ray micro-computed tomography

Micro-CT images were obtained by killing brain tumour-bearing nude mice injected with EG_2-hFc sdAb for 72 h, by intracardiac perfusion of the blood with heparin-treated saline, followed by infusion of a radiopaque silicone polymer as a blood pool contrast agent (Microfil MV-122, Flow Tech, Carver, MA, USA), which was left to polymerize overnight, followed by fixing in 10% formalin. In preparation for scanning with micro-CT, the brains were removed from the skulls and mounted in 1% agar. Each image was acquired over 900 projection views through 360° rotation, and three-dimensional CT images were reconstructed with $16 \times 16 \times 16$-μm^3 voxels using a GE eXplore Locus SP Specimen Scanner (GE Healthcare Biosciences, London, ON, Canada) at 16 μm isotropic resolution (at 80 kVp, 80 μA, 2000 ms integration time). This instrument emits X-rays, which are filtered to remove low-energy photons, and are transmitted through the sample and detected using a CsI scintillating material, and finally imaging is performed using a charge-coupled device. Each of the 900 projection images was the average of four separate frames to improve the signal to noise ratio. Total brain scan time was approximately 3 h.

Co-registration of injected EG_2-hFc-cy5.5 (optical imaging) and Microfil-perfused brain (micro-CT imaging)

CT-fusion volume was generated with the OptiView™ CT-Fusion software module (ART, Advanced Research Technologies Inc.) and exported in DICOM format for co-registration using AMIRA®, a 3D biomedical visualization software analysis tool from Visage Imaging™ (San Diego, CA, USA). The co-registration technique employed by OptiView™ matches the X-ray fiducial markers that appear on micro-CT images with software markers that are inserted at predetermined positions into the optical image volume slices. AMIRA® software was then used to co-register and visualize the optical and CT images.

Immunofluorescence analyses of brain and tumour sections

After completion of the *in vivo* brain tumour targeting experiments, animals were perfused with heparin-treated saline, their brains dissected and then frozen on dry ice. Mouse brain tissues were embedded in a Tissue-Tek freezing medium and sectioned on a cryostat at 10 μm thickness, then mounted on Superfrost Plus microscope slides (Fisher Scientific Company, Ottawa, ON, Canada). Frozen tissue sections were fixed in methanol for 10 min at room temperature (r.t.). Slides were rinsed with 0.2 M PBS (pH 7.3), followed by incubation with 5% goat serum in PBS for 1 h with 0.1% Triton-X 100 at r.t. After being blocked, the slides were incubated with rat anti-mouse CD31 primary antibody (1:100) for 1 h at r.t. followed by $Alexa^{488}$-labelled goat anti-rat secondary (1:300; Invitrogen Corporation, Carlsbad, CA, USA) for 1 h at r.t. Slides were again washed with PBS five times, dried of excess liquid and then mounted on cover slips using DAKO fluorescent mounting media containing Hoechst (1:1000; Dako Canada, Mississauga, ON, Canada).

Frozen human brain tumour specimens classified according to the WHO classification scheme for brain tumours (Dr Garnette Sutherland, Foothills Medical Center, Calgary, AB, Canada) were embedded in Tissue-Tek freezing medium and sectioned on a cryostat at 10 μm thickness, then mounted on Superfrost Plus microscope slides. Sections were fixed in methanol for 10 min, permeated with 0.1% Triton-X for 10 min and then incubated with 5% donkey serum for 1 h. After being blocked, the slides were incubated with a polyclonal rabbit anti-EGFR antibody (1:300, Santa Cruz Biotechnology, Santa Cruz, CA, USA) for 1 h at r.t. Sections were then washed three times with PBS, before incubation with secondary antibody, goat anti-rabbit $Alexa^{647}$ (1:500; Molecular Probes) for 1 h at r.t. Alternatively, slides were also incubated with the pentavalent V2C-EG_2 sdAb (1:100) for 3 h at r.t. These sections were then washed three times with PBS, followed by incubation with rabbit polyclonal anti-verotoxin antibody (1:300, custom-made in-house) for 1 h. Sections

were again washed five times with PBS and then incubated with secondary antibody, goat anti-rabbit Alexa^{647} (1:500) for 1 h at r.t. Both anti-EGFR-labelled and V2C-EG_2 sdAb-labelled sections were further washed with PBS five times, and incubated with I lectin (ULEX; 1:20; Vector Laboratories, Burlington, ON, Canada), which stains human vascular endothelium for 3 min at r.t. Slides were then mounted using DAKO fluorescent mounting reagent containing Hoechst (1:1000). In control slides, the primary antibody was omitted. Images were captured using an Olympus 1X81 inverted motorized microscope (Markham, ON, Canada) and analysed using ImagePro 6.2 (Markham, ON, Canada).

Statistical analysis

All data are reported as mean ± SEM and the differences between the groups were determined using two-way ANOVA followed by Bonferoni *post hoc* test for *in vivo* imaging. Differences greater than $P < 0.05$ were considered significant.

Results

Comparison of binding kinetics by SPR

The affinity of EG_2 sdAb for the EGFRvIII-ECD was determined by flowing serial dilutions of EG_2 over a sensor chip surface on which EGFRvIII-ECD was immobilized. The sensorgrams were fit globally to a 1:1 Langmuir binding model using the BiaEvaluation software that is based on numerical integration (Figure 2A). The resulting equilibrium dissociation constant (K_D) was calculated to be $9.7 \pm 0.7 \times 10^{-8}$ M ($n = 9$), which is similar to the affinity of EG2 for binding to EGFR-ECD ($K_D = 5.5 \times 10^{-8}$ M) that was reported previously (Bell *et al*., 2009). It is not surprising that EG_2 can bind to both EGFR-ECD and EGFRvIII-ECD since the amino acid sequence of EGFRvIII is a subset of that in EGFR-ECD, and since no selective pressure against EGFR-ECD binders was applied during the panning process (Bell *et al*., 2009).

Multimerization of sdAbs into higher valency constructs has been shown to significantly increase their apparent affinity due to avidity effects (Cortez-Retamozo *et al*., 2002; Zhang *et al*., 2004). In this study, the binding of monovalent (EG_2), bivalent (EG_2-hFc) and pentavalent (V2C-EG_2) constructs was compared. In the first experimental design, the binding behaviour of the three sdAb formats was monitored by flowing serial dilutions of the antibodies over three EGFRvIII-ECD surfaces with different receptor densities, ranging from 300 RU to 1400 RU. Figure 2B–D display the normalized sensorgrams obtained from the 0.5 μM injections of the three forms of EG_2 over the three EGFRvIII-ECD surfaces. As expected for a monovalent binder that does not exhibit avidity effects, the EG_2 sensorgrams were not affected by receptor surface density (Figure 2B). In contrast, as expected when avidity is occurring, the apparent affinities of the multivalent constructs increased with increasing amounts of EGFRvIII-ECD on the surface, due to decreases in apparent dissociation rates (Figure 2C,D). To validate that these differences in dissociation rates are due to avidity effects, the experimental design was reversed, with the three antibody constructs being immobilized on individual surfaces and EGFRvIII-ECD (which is intrinsically monomeric) being injected. The shapes of the normalized sensorgrams of the 0.5 μM injections over the three different surfaces are similar, as is expected in the absence of avidity. A slightly slower k_a and faster k_d was observed for the V2C-EG_2. These results show that the binding unit (monomeric EG_2) on all antibody formats has an essentially identical intrinsic affinity to the target and that changes in apparent affinity must be attributed to multivalency. These observations are similar to those from our previous experiments in which the interactions of the three EG2 sdAb constructs to EGFR-ECD surfaces were examined (Bell *et al*., 2009).

Fitting the data derived from the first experimental design, that is, when multivalent constructs were flowing over immobilized target, to a 1:1 model provides an estimate of the gain in apparent affinity achieved under the given experimental conditions. Figure 2F illustrates the association rates and dissociation rates calculated for EG_2, EG_2-hFc and V2C-EG_2 binding to the three different EGFRvIII-ECD surface densities (Figure 2B–D show sensorgrams for only 0.5 μM; however, the rate constants shown in Figure 2F were derived from global fitting of data that included additional concentrations of antibodies). As expected, while the association rates did not change as a function of receptor density, a significant decrease in dissociation rates with increasing surface density was observed for the multivalent constructs, but not for monovalent EG_2. To further illustrate the gain in apparent affinity achieved as a result of multivalency and avidity, we calculated the enhancement factor β, which is the ratio of equilibrium binding constants of the multivalent and monovalent binders ($\beta = K_A^N/K_A^{mono}$; Mammen *et al*., 1998). For the binding to the three EGFRvIII-ECD surfaces, we obtained enhancements of $\beta_{EG2\text{-}hFc}$ = 50–600 and $\beta_{V2C\text{-}EG2}$ = 10–40, with the greater enhancement occurring on the higher density surfaces. These results agree with those from previous studies on multivalent binding, which demonstrated that the enhancement factor is proportional to the epitope surface density (see review by Pluckthun and Pack, 1997).

To evaluate the binding of EG_2 to full-length receptors on the plasma membrane of U87MG cells overexpressing EGFR or EGFRvIII, affinity labelling and competition binding assays with radiolabelled EG_2 were performed. The affinity labelling results (Figure 3A) demonstrate specificity of [^{125}I]-EG2 binding to EGFR and EGFRvIII, since bands of the expected molecular weights were labelled, and this labelling was competed for by excess unlabelled EG2. Figure 3B,C show the binding experiments on the EGFR or EGFRvIII overexpressing U87MG cells, respectively, in which [^{125}I]-EG2 was competed with unlabelled EG2. The [^{125}I]-EG_2 cell binding data were fit to a one-site competition model using non-linear regression analysis, which allows for the calculation of the IC_{50} (the half-maximal inhibitory concentration). Since in our experimental setting the concentration of labelled EG_2 was far below its K_D (as determined by SPR experiments), the apparent affinity (K_i) is expected to be similar to the IC_{50} (Cheng and Prusoff, 1973). The apparent affinity for monovalent EG_2 was found to be $7.0 \pm 2.7 \times 10^{-8}$ M and $6.0 \pm 0.1 \times 10^{-8}$ M for U87MG.wtEGFR and U87MG.EGFRvIII overexpressing cells, respectively (Figure 3A,B). These affinities are very similar to those determined by SPR. Competition experiments were also

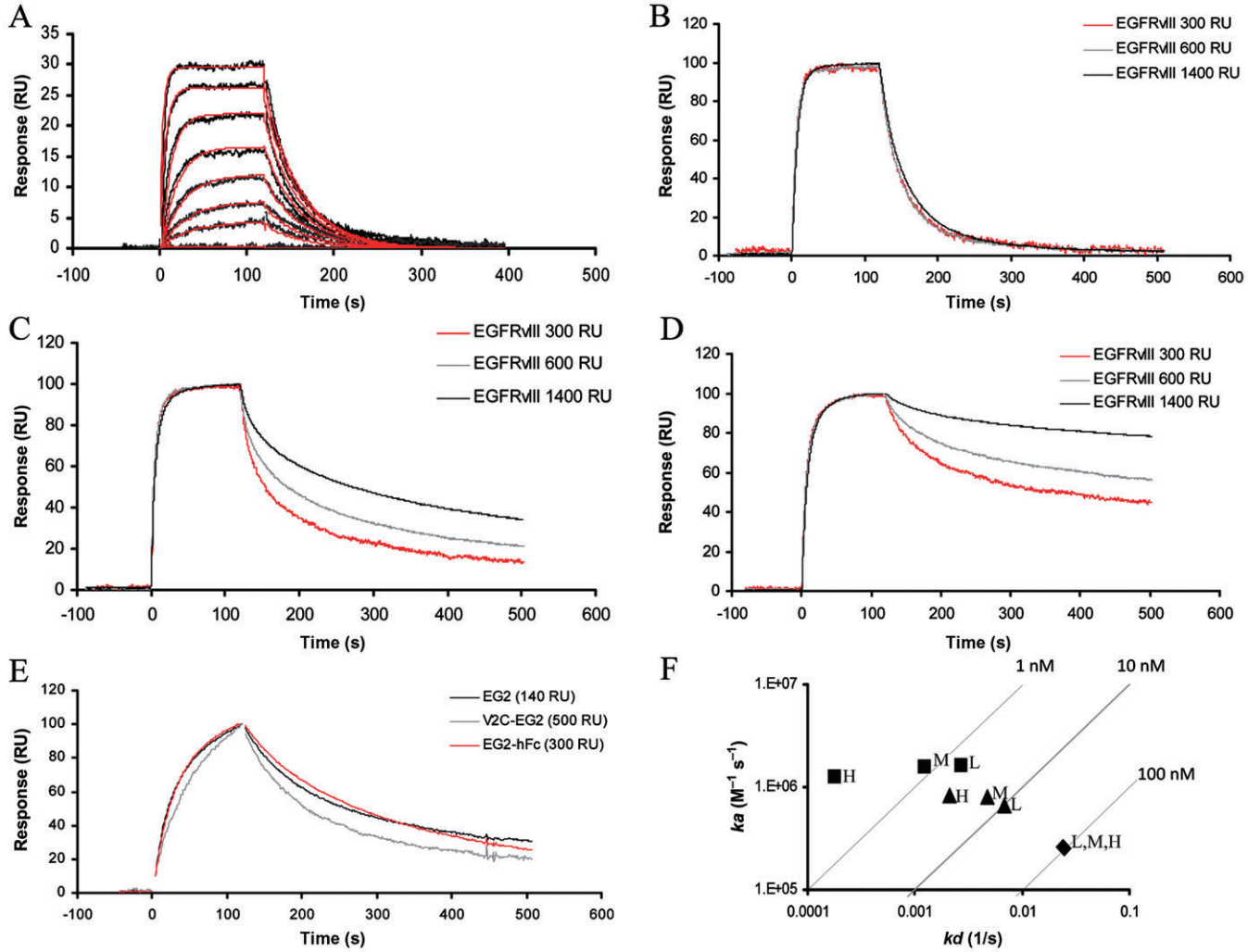

Figure 2 SPR biosensor analysis. (A) Affinity determination. EG_2 was injected for 120 s at concentrations between 7.8 nM and 500 nM over an EGFRvIII-ECD surface (300 RU) at a flow rate of 20 $\mu L \cdot min^{-1}$. The resulting sensorgrams were fitted globally to a 1:1 Langmuir binding model (shown in red). A dissociation constant (K_D) of $9.69 \pm 0.68 \times 10^{-8}$ M was derived ($k_a = 2.56 \pm 0.19 \times 10^5 \cdot M^{-1} \cdot s^{-1}$, $k_d = 2.53 \pm 0.92 \times 10^{-2} \cdot s^{-1}$). (B–D) Comparison of SPR sensorgrams obtained from surfaces with different epitope densities. EGFRvIII-ECD was immobilized at three different densities on a Biacore CM-5 chip and serial dilutions ranging from 3.7 nM to 1 μM of EG_2 (B), V2C- EG_2 (C) and EG2-hFc (D) were injected in series over the three flow cell surfaces at a flow rate of 20 $\mu L \cdot min^{-1}$. Sensorgrams were normalized to 100 RU in order to compensate for the different quantities of protein captured on the surfaces. For simplicity, only the 0.5 μM injections are plotted. (E) EG_2, V2C- EG_2 and EG_2-hFc were immobilized on surfaces and 0.5 μM EGFRvIII-ECD was injected at 30 $\mu L \cdot min^{-1}$ over the three surfaces. The resulting sensorgrams were normalized to 100 RU to allow for better comparison between the flow cells. (F) Association and dissociation rates of EG_2 (◆), EG_2-hFc (■) and V2C-EG_2 (▲) when binding to three different density EGFRvIII surfaces. The values of the kinetic constants for all three constructs were derived from fitting the data to a 1:1 Langmuir model. L (low), M (medium) and H (high) indicate the receptor density of the flow cell from which the data were obtained: low = 300 RU, medium = 600 RU and high = 1400 RU EGFRvIII-ECD, respectively. All results are representative of at least three independent experiments.

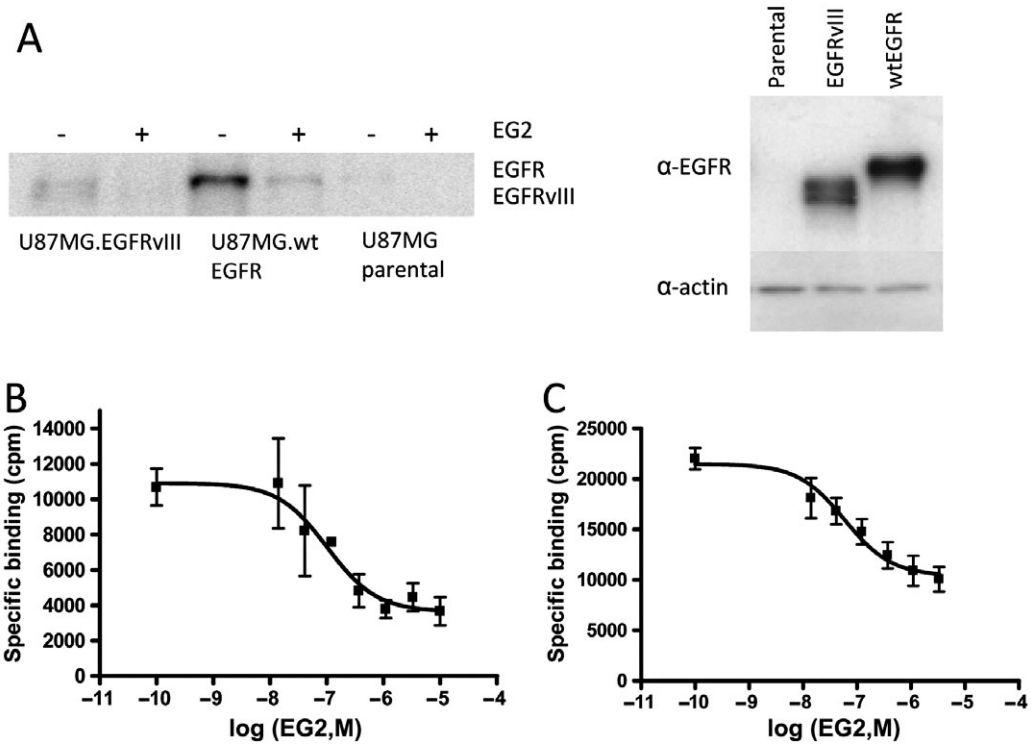

Figure 3 EGFR and EGFRvIII expressed on U87MG cell lines were affinity labelled with [^{125}I]-EG_2 in the absence and presence of 100-fold excess unlabelled EG_2 (A, left). The resulting bands were competed for by unlabelled sdAb and corresponded to the expected molecular weight as confirmed by Western blot (A, right). IC_{50} values were calculated by fitting [^{125}I]-EG_2 cell binding data to a one-site competition model using non-linear regression. For monovalent EG_2 binding to EGFR on the surface of U87MG.wtEGFR cells, the average IC_{50} was $7.04 \pm 2.67 \times 10^{-8}$ M (B). Similarly, the average IC_{50} on U87MG.EGFRvIII cells was $5.98 \pm 0.12 \times 10^{-8}$ M (C).

performed using unlabelled EG_2-hFc and V2C-EG_2 as competitors. Although these data did not fit a one-site competition model (as might be expected when avidity effects are occurring), they suggested that multivalent EG2 was competing more effectively than monomeric EG2. Also in support of avidity effects occurring at the cell surface, we observed that monomeric EG2 dissociates from cell surfaces more rapidly than multivalent EG2 (data not shown).

Pharmacokinetics and biodistribution of mono-, bi- and pentavalent EG_2 sdAbs in vivo

A two-compartment, first-order pharmacokinetic model was used to fit the serum concentration–time curves, after i.v. administration of the various sdAb constructs to the intact CD-1 mice. The pharmacokinetic parameters for EG_2-cy5.5 sdAb, V2C-EG_2-cy5.5 sdAb and EG_2-hFc-cy5.5 sdAb revealed volume of distribution (V) values of 1.5, 0.7 and 0.5 mL, respectively. This indicates that the antibodies are all mostly restricted to the vascular compartment of the mouse (total mouse blood volume is approximately 1.5 mL). The half-life of elimination (β half-life) varied greatly among the different sdAb constructs. EG_2-hFc-cy5.5 sdAb had the longest half-life of 12 h, while V2C-EG_2-cy5.5 sdAb and EG_2-cy5.5 sdAb had a much shorter $t_{1/2}$ of 70 min and 5 min, respectively. The long half-life of the EG_2-hFc sdAb in the circulation was further reflected in the slow clearance rate from the body of 0.003 mL·min^{-1} compared to 0.01 and 0.1 mL·min^{-1} for V2C-EG_2-cy5.5 sdAb and EG_2-cy5.5 sdAb, respectively.

The biodistribution of three cy5.5-labelled anti-EGFR sdAb constructs was then evaluated using *in vivo* and *ex vivo* optical imaging after they had been injected i.v. into mice bearing U87MG.EGFRvIII orthotopic brain tumours. Figure 4A shows representative whole-body *in vivo* images (top panels) and organ images *ex vivo* (bottom panels) of animals injected with 1 nmol of EG_2-hFc-cy5.5 (Figure 4A1), V2C-EG_2-cy5.5 (Figure 4A2) and EG_2-cy5.5 (Figure 4A3), 72 h after injection. Tumour signal was quantified for each antibody construct at different times after injection and is presented in Figure 4B. Analysis of the head region of interest showed that EG_2-hFc-cy5.5 sdAb accumulated gradually in the brain tumour region over time, with the maximum accumulation at 72 h reaching fluorescence concentration values of 1204 ± 222 AU, compared to 253 ± 148 AU for V2C-EG_2-cy5.5 sdAb and 104 ± 87 AU for EG_2-cy5.5 sdAb. The values for fluorescence concentration in the tumour region indicated that the EG2-cy5.5 and V2C-EG_2-cy5.5 achieved a transient increase in tumour signal only at 1 h after injection, whereas EG_2-hFc-cy5.5 achieved and maintained the highest tumour signal at 72 h, five times greater than V2C-EG_2-cy5.5 and 12 times greater than EG2-cy5.5 at this same time point (Figure 4B).

At the end of the imaging protocol, 72 h after injection of the cy5.5-labelled antibody construct, animals were perfused with saline, and their organs (liver, kidney, spleen, lung, heart, brain, muscle) were imaged *ex vivo* (Figure 4A, bottom panels). The total fluorescence concentration (FC)·g^{-1} tissue was calculated and quantified (Figure 4C) for each organ. The

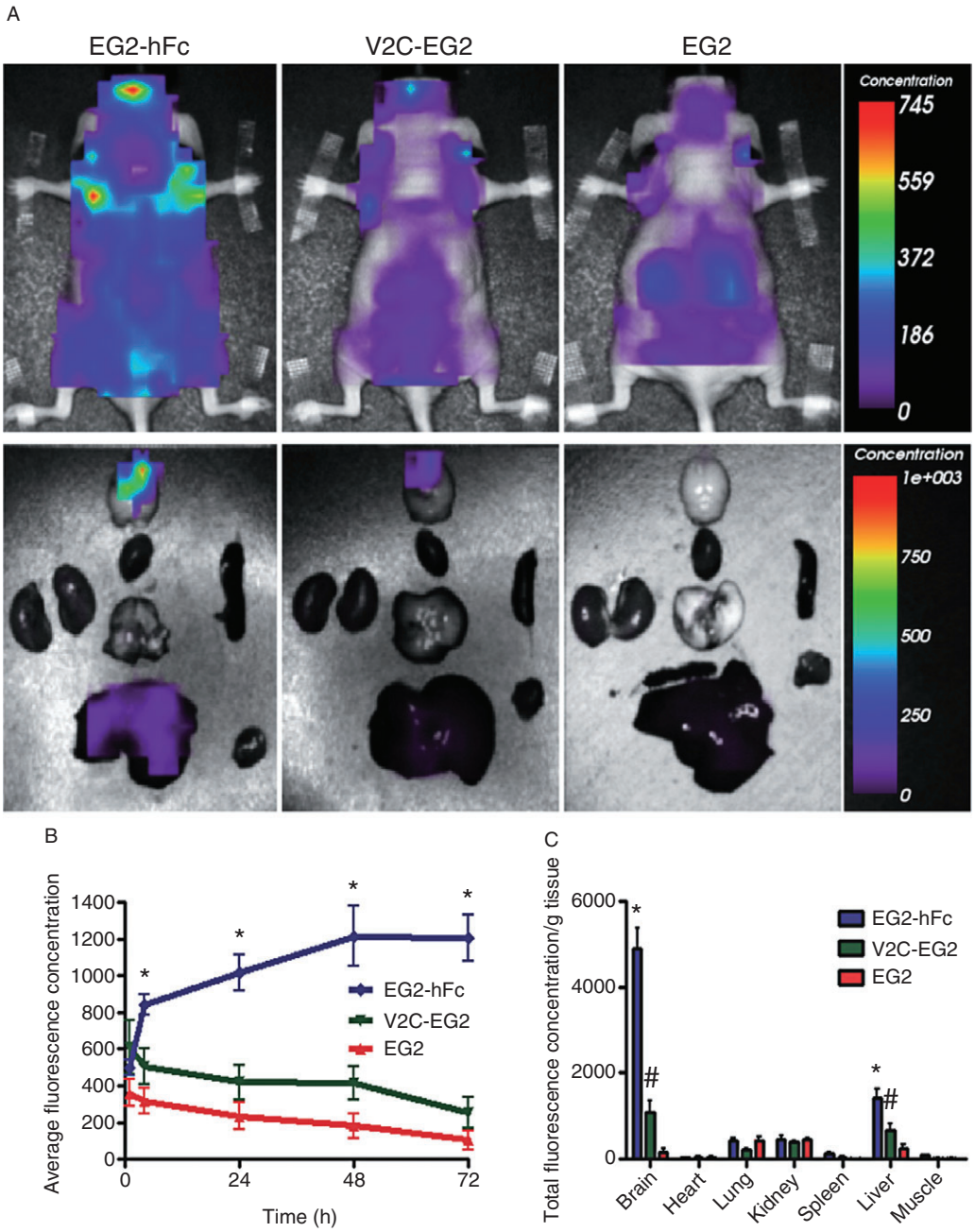

Figure 4 (A, upper panel) Dorsal whole body, *in vivo*, optical images of mice bearing U87MG.EGFRvIII brain tumours 72 h after i.v. injection of 1 nmol of cy5.5-labelled EG_2-hFc (left panel), V2C-EG_2 (middle panel) and EG_2 (right panel). (A, lower panel) *Ex vivo* optical images of organ biodistribution for EG_2-hFc (left panel), V2C-EG_2 (middle panel) and EG_2 (right panel). (B) Graph illustrating the fluorescence concentration in the brain tumour region of various sdAbs in the brain over time, analysed from optical imaging data. * Indicates significant difference between EG_2-hFc and all other sdAbs ($P < 0.05$). The data are expressed as mean ± SD for $n = 6$ animals. EG_2-hFc-cy5.5 sdAb was statistically different at 4 ($P < 0.05$), 24 ($P < 0.001$), 48 ($P < 0.001$) and 72 h ($P < 0.001$) compared to EG_2-cy5.5 sdAb and at 24 ($P < 0.05$), 48 ($P < 0.01$) and 72 h ($P < 0.01$) compared to V2C-EG_2-cy5.5 sdAb. (C) Graph illustrating the total fluorescence concentration of EG_2-hFc, V2C-EG_2 and EG_2 at 72 h in various organs. * Indicates significant difference between EG_2-hFc and all other sdAbs ($P < 0.05$), and # indicates significant difference between V2C-EG_2 and EG_2 sdAb. The data are expressed as mean ± SD for $n = 6$ animals.

total FC·g^{-1} tissue in the brain was 4893 ± 555, 1071 ± 392 and 166 ± 128 AU·g^{-1} tissue for EG_2-hFc-cy5.5, V2C-EG_2-cy5.5 and EG_2-cy5.5 sdAb, respectively (Figure 4C). The remaining concentration for all constructs in other organs was minimal at 72 h, with the exception of the liver, where both EG_2-hFc-cy5.5 and V2C-EG_2-cy5.5 showed higher FC·g^{-1} tissue compared to EG_2-cy5.5.

Co-registration of time-domain volumetric optical molecular images of EG_2-hFc sdAb with micro-CT images of brain and tumour vessels

To confirm that the *in vivo* fluorescence imaging signal with the EGFR molecular targeting agent, EG_2-hFc-cy5.5, originated from the anatomical region of the orthotopic GBM tumour, we used a co-registration paradigm with the micro-

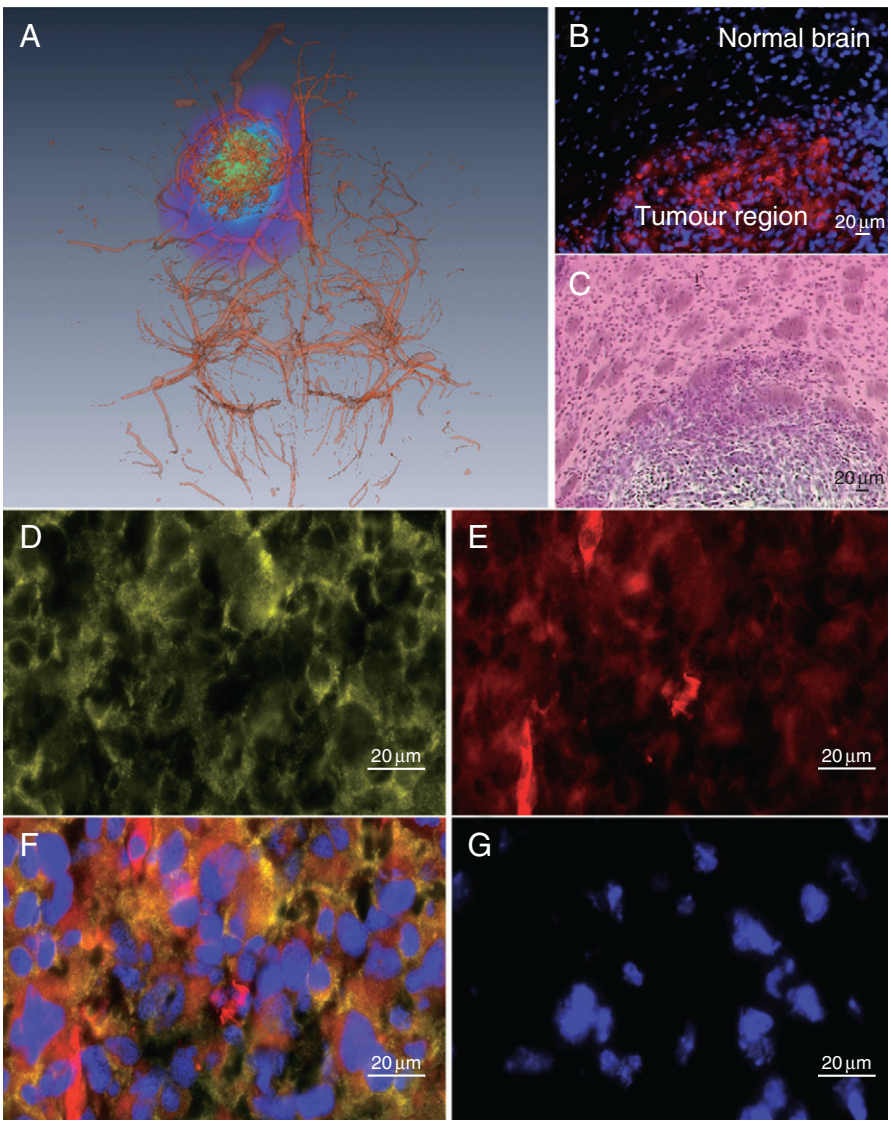

Figure 5 (A) Co-registration of time-domain volumetric optical imaging of EG_2-hFc-cy5.5 and high-resolution vascular micro-CT scanning of brain tumour at 16 μm in nude mice. (B) Fluorescence image of intravenously injected EG_2-hFc-cy5.5 (red) after 72 h in U87MG.EGFRvIII tumour-bearing mouse brain. (C) Haematoxylin and eosin staining of a brain tumour section. (F) Immunofluorescent image of the co-localization (orange) of EGFR expression (D, yellow) with injected EG_2-hFc-cy5.5 (E, red) after 72 h in a section of a U87MG.EGFRvIII tumour-bearing mouse brain. (G) Lack of EGFR expression or EG_2-hFc-cy5.5 signal in normal brain. Scale bar: 20 μm.

CT-derived anatomical images of brain and brain tumour vasculature. Since brain tumour parenchyma does not have sufficient CT contrast properties for anatomical delineation from the normal brain tissue, we used a vascular casting technique to contrast enhance brain/brain tumour vasculature prior to co-localization with the molecular optical image. Tumour vasculature is known to be denser and anatomically abnormal and could therefore provide 'anatomical reference' for brain tumour. The vascular casting technique that uses a radiopaque silicone polymer Microfil and *post-mortem* imaging provided detailed brain tumour vascular anatomy at sizes down to 16 μm diameter (Figure 5A). The anatomical region of the orthotopic brain tumour was clearly demarcated by a vascular network of high-density and irregular branching. The optical image of EG_2-hFc-cy5.5 sdAb obtained in the same animal at 24 h co-registered within the same anatomical region occupied by abnormal tumour vasculature visualized by micro-CT (Figure 5A).

Ex vivo *fluorescent microscopy of injected EG_2-hFc-cy5.5 in U87MG.EGFRvIII brain tumours*

In addition to anatomical co-localization of molecular optical signal with brain tumour 'proper', cellular co-localization of the injected EG_2-hFc-cy5.5 sdAb with respect to EGFR-expressing tumour cells was carried out by immunofluorescence in brain sections after the end of imaging protocol (72 h after injection). EG_2-hFc-cy5.5 fluorescence was detected in a diffuse pattern throughout the tumour region (Figure 5B) characterized by high nuclear/cellular density (Figure 5C). In contrast, no cy5.5 fluorescence was detected in either tumour surrounding ispilateral brain or in the contralateral brain

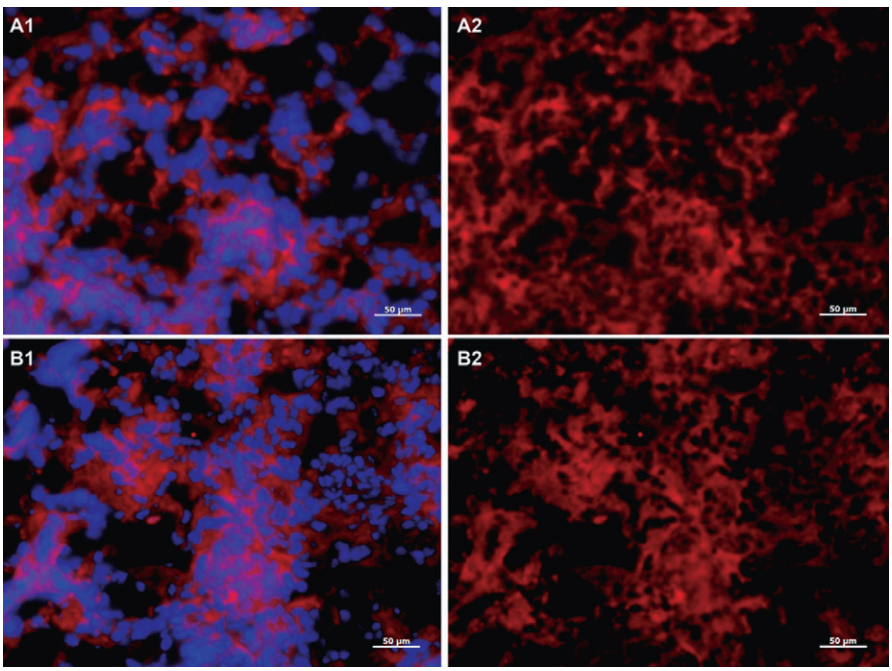

Figure 6 (A1) Immunofluorescence of anti-EGFR polyclonal antibody or (B1) V2C-EG_2 sdAb on sections of human high-grade glioma brain tumour. EGFR expression in red, DAPI staining for cell nuclei in blue and ULEX staining for brain blood vessels in green. EGFR expression only (in red) is shown in right panels (A2, B2). Scale bar: 50 µm.

hemisphere (Figure 5B,G). Co-localization of the EG_2-hFc-cy5.5 signal (Figure 5E) with EGFR expression (Figure 5D) demonstrated that the EG_2-hFc-cy5.5 extravasated into the tumour parenchyma and could interact with its receptor (Figure 5F).

Detection of EGFR in human brain tumour tissue sections using pentameric V2C-EG_2 sdAb

The ability of anti-EGFR sdAb to detect EGFR in human high-grade glioma tumour tissue sections was also evaluated. The V2C-EG_2 was applied *ex vivo* to sections of tumour tissue, followed by immunohistochemical detection using an anti-verotoxin subunit B1 rabbit polyclonal antibody that selectively targets the verotoxin subunit scaffold in the pentameric structure of V2C-EG_2. The specificity of the binding of V2C-EG_2 was validated using a commercially available anti-EGFR polyclonal antibody in human high-grade glioma tissue, which detected widespread expression of EGFR (Figure 6A). V2C-EG_2 when used as a primary antibody produced a similar staining pattern to that of the commercially available anti-EGFR polyclonal antibody (Figure 6B). This experiment confirms that anti-EGFR sdAb constructs recognize EGFR in human glioblastomas.

Discussion and conclusions

In this study the tumour-targeting properties of various anti-EGFR/EGFRvIII sdAb constructs were tested for their potential use as molecular imaging agents in high-grade glioblastoma tumours. EG_2 (monovalent, 15 kDa), EG_2-hFc (bivalent, 80 kDa) and V2C-EG_2 (pentavalent. 128 kDa) were assessed by comparing their binding affinities for EGFR/EGFRvIII receptor ectodomains and for EGFR/EGFRvIII-expressing cells *in vitro*, and their pharmacokinetic, biodistibution and tumour localization/retention behaviours *in vivo*. It was demonstrated that the EG_2-hFc sdAb construct had the highest apparent affinity for the EGFR/EGFRvIII receptor(s), the longest circulation half-life and the best glioblastoma-targeting properties among the three constructs tested, suggesting that it can be developed into a molecular imaging and/or therapeutic agent for EGFR-overexpressing tumours, including glioblastomas.

An ideal antibody-based targeted imaging agent should be able to penetrate the tumour mass, and bind to tumour cells expressing the target with sufficient affinity to be retained in the tumour and to produce a detectable tumour to background tissue signal ratio. At the same time, it should clear from the circulation relatively quickly to enable detection by imaging in a reasonable time after contrast administration. In contrast, for a therapeutic antibody, a long circulation half-life combined with high affinity for the target is generally preferred to avoid excessive repeat dosing and to achieve therapeutic effect.

By SPR biosensor analysis, EG_2 sdAb exhibited low nanomolar affinity for the immobilized extracellular domains of EGFR and EGFRvIII (55 nM and 97 nM, respectively). The estimated K_D values for the cell-based competition binding data for EG_2 were approximately 70 nM and 60 nM for EGFR and EGFRvIII, respectively, in good agreement with the values determined by SPR. SPR analysis also demonstrated that multimerization of the EG_2 sdAb into a bivalent or pentavalent format, EG2-hFc or V2C-EG_2, increased the avidity for EGFRvIII as evidenced by a decreased kinetic off-rate. The bivalent EG2-hFc sdAb demonstrated the highest avidity, suggesting that a favourable orientation of the binding

domains within the construct is an important parameter. It is likely that the hinge region of the bivalent sdAb affords greater flexibility in the molecule allowing for the simultaneous binding to two receptors, which then results in avidity.

It has been demonstrated previously that the apparent affinity of bivalent sdAb constructs can increase from 10- to 500-fold compared to their monovalent sdAb counterparts (Coppieters *et al*., 2006; Roovers *et al*., 2007). Bivalent EG_2-hFc and pentavalent V2C-EG_2 showed an increase in apparent affinity due to avidity of 50- to 600- and 10- to 40-fold, respectively, pushing the affinity of these sdAb constructs into the low or even sub-nM range, depending on receptor density. In comparison, the mAb, cetuximab, has a reported apparent affinity of 1.1 nM for EGFRvIII as determined by SPR (Patel *et al*., 2007) while a single-chain Fv (scFv) achieved an affinity of 1.5 nM for EGFRvIII (Kuan *et al*., 2000). It is important to note that very high affinity (in the picomolar range) can also impair tumour penetration by preventing the antibody from reaching all tumour cells (Adams GP *et al*., 2001). For an scFv against HER-2 with affinities that varied from 10^{-7} to 10^{-11}, it was demonstrated that the lower affinity formats exhibited more diffuse tumour targeting compared to the highest affinity formats, which remained in the perivascular areas only and could not penetrate deeper into tumour parenchyma (Adams GP *et al*., 2001).

In vivo, the pharmacokinetic profiles demonstrated short plasma half-lives and fast clearance rates for EG_2 (41 min) and V2C-EG_2 (86 min) and a long plasma half-life and slow clearance rate for EG_2-hFc (12 h). The reason that V2C-EG_2 (128 kDa) exhibits only a marginal increase in plasma half-life compared to EG_2 (15 kDa) despite its higher molecular weight is likely to be due to the presence of protease cleavage sites in the VTB1 scaffolding protein and its low stability in plasma. In contrast, EG_2-hFc (80 kDa) is resistant to protease degradation and demonstrated a prolonged plasma half-life consistent with a lack of kidney filtration.

The biodistribution of cy5.5 labelled EG_2, EG_2-hFc and V2C-EG_2 in U87MG.EGFRvIII tumour-bearing mice indicated that while EG_2 and V2C-EG_2 transiently accumulated in tumours only at very early time points (~1 h) followed by low retention, the EG_2-hFc sdAb displayed high brain tumour accumulation, reaching near maximum levels as early as 4 h, and persisted in the tumour for at least 72 h. The molecular–anatomical co-registration protocols used in this study enabled a 3D reconstruction of fluoroprobe concentration linked to tissue depth by time-domain optical imaging and a detailed presentation of the contrast-enhanced microvascular architecture in brain tumour by micro-CT. Cy5.5 signal of EG_2-hFc co-registered spatially with the dense, tortuous blood vessels delineating anatomical tumour boundaries within the brain tissue. The immunofluorescence analyses in brain sections further suggested that EG2-hFc extravasated permeable tumour vessels and diffusely penetrated tumour interstitial space.

Uniform tumour penetration remains a challenge for antibody targeting. In the brain tumour, the high interstitial pressure and dense extracellular matrix will limit the penetration of proteins, including monoclonal antibodies (Jain, 1994; Schier *et al*., 1996). A smaller antibody size could enhance the penetration of the targeting agent compared to larger molecules (Colcher *et al*., 1998). EG_2-hFc (80 kDa) is a smaller construct compared to both cetuximab (150 kDa) and scFv-Fc (105 kDa), which may lead to improved brain tumour localization. The superior tumour retention of EG_2-hFc after it has entered the tumour region is probably due to its high affinity binding to the tumour target, since there was still a maximal signal present 72 h after complete clearance of EG_2-hFc from the body. Therefore, the superior tumour-targeting capacity of EG_2-hFc compared to EG_2 and V2C-EG_2 is attributed to combined effects of moderate molecular size, increased avidity and, most important, its long plasma half-life (Khawli *et al*., 2003). Despite being suboptimal for *in vivo* tumour targeting due to its short plasma half-life, the pentameric V2C-EG_2 construct demonstrated excellent reactivity against EGFR/EGFRvIII in immunofluorescence assays, comparable to a commercial IgG antibody.

Other strategies have also been employed to increase the short serum half-lives of sdAbs, including conjugation of polyethylene glycol chains (Chapman *et al*., 1999; Lu *et al*., 2007) and design of bi-specific sdAbs that target the long-circulating serum protein, albumin (Roovers *et al*., 2007) or immunoglobulin (Harmsen *et al*., 2005), leading to circulation half-lives in the order of 2 days and 9 days, respectively. In another study, which used five different Fc variants, a spectrum of half-lives ranging from 8 h to 12 days for scFv-Fc (105 kDa) antibodies was obtained (Kenanova *et al*., 2007). The site-specific mutation of the neonatal Fc receptor-binding region of the Fc on antibodies can also significantly regulate their pharmacokinetic behaviour (Roopenian and Akilesh, 2007). The presence of a human Fc on the EG_2-hFc sdAb opens the door for future optimization of this construct as a therapeutic agent, in that modifications (mutations) of this region could increase circulation half-lives to lengths more appropriate for therapeutic applications and Fc could participate in the activation of Fc-dependent cytotoxic events (Clynes *et al*., 2000).

In clinical GBMs, a concomitant overexpression of EGFR and EGFRvIII is frequently observed (Wikstrand *et al*., 1998). Since EG_2 sdAb can recognize both the EGFR and EGFRvIII it could be used for targeting GBMs and other cancers expressing either or both types of EGFR, including head and neck squamous cell cancer, cervical, renal cell, lung, prostate, bladder, colorectal, pancreatic and breast cancer (Kuan *et al*., 2001). However, there is a potential for non-specific accumulation of the molecular imaging agent in EGFR-negative tumours, which could be due to several factors such as tumour vascularization or necrosis (which may interfere with tracer uptake; Pantaleo *et al*., 2009). With optimization it is expected that these imaging agents will not retain (bind) to the EGFR-negative GBM tumours.

In conclusion, this study demonstrates that a significant gain in apparent affinity and prolongation of half-life of EGFR-targeting single-domain antibody fragments can be achieved through fusion/dimerization of the V_HH-fragment with an Fc domain. The EG_2-hFc construct demonstrates an effective molecular targeting of intracranial brain tumours in *in vivo* molecular imaging applications due to the balance achieved among high apparent affinity, improved serum half-life, intermediate molecular size and good tumour penetration.

Acknowledgements

The authors would like to thank Drs Y. Durocher, P. Picot, A. Bell, J. Baardsnes, M. Jaramillo, S. Grothe and D. Fatehi for their technical assistance and useful discussions. We would also like to thank Mr T. Devesceri for his help with graphic and image processing. This work was supported by a Canadian Institutes of Health Research team grant for molecular imaging of brain tumours.

Conflict of interest

None to declare.

References

Abulrob A, Giuseppin S, Andrade MF, McDermid A, Moreno M, Stanimirovic D (2004). Interactions of EGFR and caveolin-1 in human glioblastoma cells: evidence that tyrosine phosphorylation regulates EGFR association with caveolae. *Oncogene* **23**: 6967–6979.

Abulrob A, Sprong H, Van Bergen en Henegouwen P, Stanimirovic D (2005). The blood-brain barrier transmigrating single domain antibody: mechanisms of transport and antigenic epitopes in human brain endothelial cells. *J Neurochem* **95**: 1201–1214.

Abulrob A, Brunette E, Slinn J, Baumann E, Stanimirovic D (2007). In vivo time domain optical imaging of renal ischemia-reperfusion injury: discrimination based on fluorescence lifetime. *Mol Imaging* **6**: 304–314.

Abulrob A, Brunette E, Slinn J, Baumann E, Stanimirovic D (2008). Dynamic analysis of the blood-brain barrier disruption in experimental stroke using time domain in vivo fluorescence imaging. *Mol Imaging* **7**: 248–262.

Adams GP, Schier R, McCall AM, Simmons HH, Horak EM, Alpaugh RK *et al*. (2001). High affinity restricts the localization and tumor penetration of single-chain Fv antibody molecules. *Cancer Res* **61**: 4750–4755.

Arbabi Ghahroudi M, Desmyter A, Wyns L, Hamers R, Muyldermans S (1997). Selection and identification of single domain antibody fragments from camel heavy-chain antibodies. *FEBS Lett* **414**: 521–526.

Belda-Iniesta C, Carpeno JC, Saenz EC, Gutierrez M, Perona R, Baron MG (2006). Long term responses with cetuximab therapy in glioblastoma multiforme. *Cancer Biol Ther* **5**: 912–914.

Bell A, Wang ZJ, Arbabi-Ghahroudi M, Chang TA, Durocher Y, Trojahn U *et al*. (2009). Differential tumor-targeting abilities of three single-domain antibody formats. *Cancer Lett* **289**: 81–90.

Blasberg RG, Groothius DR (1986). Chemotherapy of brain tumors: physiological and pharmacokinetic considerations. *Semin Oncol* **13**: 70–82.

Blick SK, Scott LJ (2007). Cetuximab: a review of its use in squamous cell carcinoma of the head and neck and metastatic colorectal cancer. *Drugs* **67**: 2585–2607.

Bolton AE, Hunter WM (1973). The labelling of proteins to highly specific radioactivities by conjugation to a 125I-containing acylating agent. *Biochem J* **133**: 529–539.

Brown PM, Debanne MT, Grothe S, Bergsma D, Caron M, Kay C *et al*. (1994). The extracellular domain of the epidermal growth factor receptor. Studies on the affinity and stoichiometry of binding, receptor dimerization and a binding-domain mutant. *Eur J Biochem* **225**: 223–233.

Campa MJ, Kuan CT, O'Connor-McCourt MD, Bigner DD, Patz EF Jr (2000). Design of novel small peptide targeted against a tumor-specific receptor. *Biochem Biophys Res Commun* **275**: 631–636.

Chapman AP, Antonivw P, Spitali M, West S, Stephens S, King DJ (1999). Therapeutic Antibody fragments with prolonged in vivo half-lives. *Nat Biotechnol* **17**: 780–783.

Cheng Y, Prusoff WH (1973). Relationship between the inhibition constant (K1) and the concentration of inhibitor which causes 50 per cent inhibition (I50) of an enzymatic reaction. *Biochem Pharmacol* **22**: 3099–3108.

Clynes RA, Towers TL, Presta LG, Ravetch JV (2000). Inhibitory Fc receptors modulate in vivo cytoxicity against tumor targets. *Nat Med* **6**: 443–446.

Colcher D, Pavlinkova G, Beresford G, Booth BJ, Choudhury A, Batra SK (1998). Pharmacokinetics and biodistribution of genetically-engineered antibodies. *Q J Nucl Med* **42**: 225–241.

Conrath KE, Lauwereys M, Wyns L, Muyldermans S (2001). Camel single-domain antibodies as modular building units in bispecific and bivalent constructs. *J Biol Chem* **276**: 7346–7350.

Coppieters K, Dreier T, Silence K, de Haard H, Lauwereys M, Casteels P *et al*. (2006). Formatted anti-tumor necrosis factor alpha VHH proteins derived from camelids show superior potency and targeting to inflamed joints in a murine model of collagen-induced arthritis. *Arthritis Rheum* **54**: 1856–1866.

Cortez-Retamozo V, Lauwereys M, Hassanzadeh GG, Gober M, Conrath K, Muyldermans S *et al*. (2002). Efficient tumor targeting by single-domain antibody fragments of camels. *Int J Cancer* **98**: 456–462.

De Vries NA, Beijnen JH, Boogerd W, van Tellingen O (2006). Blood-brain barrier and chemotherapeutic treatment of brain tumors. *Expert Rev Neurother* **6**: 1199–1209.

Hamers-Casterman C, Atarhouch T, Muyldermans S, Robinson G, Hamers C, Songa EB *et al*. (1993). Naturally occurring antibodies devoid of light chains. *Nature* **363**: 446–448.

Harmsen MM, Van Solt CB, Fijten HP, Van Setten MC (2005). Prolonged in vivo residence times of llama single-domain antibody fragments in pigs by binding to porcine immunoglobulins. *Vaccine* **23**: 4926–4934.

Jain RK (1994). Barriers to drug delivery in solid tumors. *Sci Am* **271**: 58–65.

Kenanova V, Olafsen T, Williams LE, Ruel NH, Longmate J, Yazaki PJ *et al*. (2007). Radioiodinated versus radiometal-labeled anti-carcinoembryonic antigen single-chain Fv-Fc antibody fragments: optimal pharmacokinetics for therapy. *Cancer Res* **67**: 718–726.

Khawli LA, Biela B, Hu P, Epstein AL (2003). Comparison of recombinant derivatives of chimeric TNT-2 antibody for the radioimaging of solid tumors. *Hybrid Hybridomics* **22**: 1–9.

Kuan CT, Wikstrand CJ, Archer G, Beers R, Pastan I, Zalutsky MR *et al*. (2000). Increased binding affinity enhances targeting of glioma xenografts by EGFRvIII-specific scFv. *Int J Cancer* **88**: 962–969.

Kuan CT, Wikstrand CJ, Bigner DD (2001). EGF mutant receptor vIII as a molecular target in cancer therapy. *Endocr Relat Cancer* **8**: 83–96.

Laskin JJ, Sandler AB (2004). Epidermal growth factor receptor: a promising target in solid tumors. *Cancer Treat Rev* **30**: 1–17.

Libermann TA, Nusbaum HR, Razon N, Kris R, Lax I, Soreq H *et al*. (1985). Amplification, enhanced expression and possible rearrangement of EGF receptor gene in primary human brain tumors of glial origin. *Nature* **313**: 144–147.

Liu TF, Tatter SB, Willingham MC, Yang M, Hu JJ, Frankel AE (2003). Growth factor receptor expression varies among high-grade gliomas and normal brain: epidermal growth factor receptor has excellent properties for interstitial fusion protein therapy. *Mol Cancer Ther* **2**: 783–787.

Lu Y, Harding SE, Turner A, Smith B, Athwal DS, Grossmann JG *et al*. (2007). Effect of PEGylation on the solution conformation of antibody fragments. *J Pharm Sci* **97**: 2062–2079.

McCafferty J, Griffiths AD, Winter G, Chiswell DJ (1990). Phage antibodies: filamentous phage displaying antibody variable domains. *Nature* **348**: 552–554.

Mammen M, Choi S-K, Whitesides GM (1998). Polyvalent interactions

in biological systems: implications for design and use of multivalent ligands and inhibitors. *Angew Chem Int Ed* **37**: 2754–2794.

Nicholas MK, Lukas RV, Jafri NF, Faoro L, Salgia R (2006). Epidermal growth factor receptor – mediated signal transduction in the development and therapy of gliomas. *Clin Cancer Res* **12**: 7261–7270.

Pantaleo MA, Nannini M, Maleddu A, Fanti S, Nanni C, Boschi S *et al*. (2009). Experimental results and related clinical implications of PET detection of epidermal growth factor receptor (EGFr) in cancer. *Ann Oncol* **20**: 213–226.

Patel D, Lahiji A, Patel S, Franklin M, Jimenez X, Hicklin DJ *et al*. (2007). Monoclonal antibody cetuximab binds to and down-regulates constitutively activated epidermal growth factor receptor vIII on the cell surface. *Anticancer Res* **27**: 3355–3366.

Pluckthun A, Pack P (1997). New protein engineering approaches to multivalent and bispecific antibody fragment. *Immunotechnology* **3**: 83–105.

Roopenian DC, Akilesh S (2007). FcRn: the neonatal Fc receptor comes of age. *Nat Rev Immunol* **7**: 715–725.

Roovers RC, van Dongen GA, van Bergen en Henegouwen PM (2007). Nanobodies in therapeutic applications. *Curr Opin Mol Ther* **9**: 327–335.

Schier R, McCall A, Adams GP, Marshall KW, Merritt H, Yim M *et al*. (1996). Isolation of picomolar affinity anti-c-erbB-2 single-chain Fv by molecular evolution of the complentarity determining regions in the centre of the antibody binding site. *J Mol Biol* **263**: 551–567.

Shinojima N, Tada K, Shiraishi S, Kamiryo T, Kochi M, Nakamura H *et al*. (2003). Prognostic value of epidermal growth factor receptor in patients with glioblastoma multiforme. *Cancer Res* **63**: 6962–6970.

Stragliotto G, Vega F, Stasiecki P, Gropp P, Poisson M, Delattre JY (1996). Multiple infusions of anti-epidermal growth factor receptor (EGFR) monoclonal antibody (EMD 55, 9000) in patients with recurrent malignant gliomas. *Eur J Cancer* **32**: 636–640.

Strupp R, Mason WP, van den Bent MJ, Weller M, Fisher B, Taphoorn MJ *et al*. (2005). Radiotherapy plus concomitant and adjuvant temozolomide for glioblastoma. *N Engl J Med* **352**: 987–996.

Vajkoczy P, Schilling L, Ullrich A, Schmiedek P, Menger MD (1998). Characterization of angiogenesis and microcirculation of high-grade glioma: an intravital multifluorescence microscopic approach in the athymic nude mouse. *J Cereb Blood Flow Metab* **18**: 510–520.

Wikstrand CJ, Reist CJ, Archer GE, Zalutsky MR, Bigner DD (1998). The class III variant of the epidermal growth factor receptor [EGFRvIII]: characterization and utilization as an immunotherapeutic target. *J Neurovirol* **4**: 148–158.

Zhang J, Tanha J, Hirama T, To R, Tong-Sevinc H, Stone E *et al*. (2004). Pentamerization of single-domain antibodies from phage libraries: a novel strategy for the rapid generation of high-avidity antibody reagents. *J Mol Biol* **335**: 49–56.

Zhang J, Liu X, Bell A, To R, Baral TN, Azizi A *et al*. (2009). Transient expression and purification of chimeric heavy chain antibodies. *Protein Expr Purif* **65**: 77–82.